Published in final edited form as:
Anal Chem. 2007 September 1; 79(17): 6868–6873. doi:10.1021/ac071162h.

Novel PDMS Based Protein Preconcentration using a Nanogap Generated by Junction Gap Breakdown

Jeong Hoon Lee[†], **Seok Chung**[‡], **Sung Jae Kim**[†], and **Jongyoon Han**[*,†,‡]

†*Department of Electrical Engineering and Computer Science, Massachusetts Institute of Technology, 77 Massachusetts Avenue, Cambridge, Massachusetts 02139*

‡*Department of Biological Engineering, Massachusetts Institute of Technology, 77 Massachusetts Avenue, Cambridge, Massachusetts 02139*

Abstract

Simple and efficient sample concentration tools are the key to the application of proteomics in a biological system. In this paper, we developed a method to realize nanofluidic preconcentrator on a PDMS based microfluidic channel. The originality of our preconcentration device is the simple nanogap formation using junction gap breakdown phenomenon between two PDMS microchannels, without using any photolithography and etching techniques. From the DC current measurement, we confirm that nanogap formed between two microchannel junctions with approximately 80 nm depth. Using this device, we achieve the concentration volume of beta-phycoerythrin protein as high as 70 pL, which is 120 folds larger than that from our previous reports, with a concentration factor as high as 10^4 within 1 hour. Also we show the availability of protein preconcentration under several different buffers (phosphate, acetate) at several different pH values (pH 5 ~ pH 9).

INTRODUCTION

Interests on Lab-on-a-Chip (LOC) systems or micro- and nanofluidic systems for analyzing chemical and biological samples, have dramatically increased in the past decade.[1,2] One of the most promising fields of the application of such miniaturized systems is preconcentration of protein, since the major challenges of biosensing lies in the enhancement of detection sensitivity for highly diluted analytes. For example, biomarker proteins that are related to cancer and other diseases are present often at very low concentrations, which are challenging to detect with standard immuno-assays such as ELISA.

Several methods are currently available for providing sample preconcentration, including field-amplified sample stacking (FASS),[3,4] isotachophoresis (ITP),[5,6] solid phase extraction (SPE),[7–9] temperature gradient focusing (TGF)[10] and various electrofocusing techniques[11–12]. Recently, preconcentration schemes utilizing perm-selectivity of nanochannel was introduced by many groups. Pu and co-workers[13] experimentally demonstrated that both cationic and anionic dyes were enriched at the cathodic end of nanochannel and excluded at anodic side, when perm-selective nanochannel current is induced. Such enrichment of ions at the cathodic side was utilized for preconcentration of proteins.[14] In our group, the highest preconcentration of million fold was achieved by Wang and co-workers, based on electrokinetic trapping (utilizing depletion behavior at the anode side of the nanochannel).[15] This method is highly efficient because one can continuously trap and accumulate molecules, while enrichment behavior at the cathodic side of the nanochannel typically shows saturation. Though the

*Corresponding author. Tel: 1-617-253-2290. Fax: 1-617-258-5846. E-mail:jyhan@mit.edu.

methods that were suggested by Wang and coworkers can achieve highly efficient concentration, the volume from electrokinetic preconcentration was relatively small (~ 0.5 pL), which is not a volume compatible with most protein analysis system such as mass spectrometry, UV detection or immuno-biosensor. What is critically needed here is an increase in preconcentration sample volume for downstream coupling with various biodetection systems.

General application of nanofluidic device that utilizes nanopore system has been reported for the separation of DNA,[16] single molecule detection,[17,18] and biomolecule concentration.[13,15] Several approaches have been described for the fabrication of a nanochannel/nanopore that is essential part of the operation of nanofluidic device. These fabrication methods can be roughly categorized into several different techniques; sacrificial layer deposition/selective etching,[19–24] silicon/glass etching and bonding technique,[25–27] and techniques utilizing focused ion beam (FIB)[28,29], electron-beam lithography (EBL),[20,30] carbon nanotube (CNT),[31] nanoimprint lithography.[32–33] However, all the fabrication methods described above require micro/nanofabrication steps that are sometimes costly and time consuming. For example, one of the methods that was developed by Mao and Han for glass-glass and glass-Si bonding process for the manufacturing of nanofluidic channel needs photolithography, etching, bonding technique with both many microfabrication step and high accuracy.[25]

On the other hand, polydimethylsiloxane (PDMS) is proven to be a useful material for the disposable microfluidic devices because of its low cost and simple fabrication process. PDMS is optically transparent down to UV wavelengths (λ~230nm), biocompatible, and has a flexibility that can be beneficial for various on-chip operations.[34–36] Perhaps due to these reasons, PDMS-based microfluidic devices have gained widespread use among researchers in various fields. In addition, PDMS-based microfluidics became the main platform for cellular BioMEMS due to gas permeability of PDMS. Therefore, it would be highly desirable to enable recent nanofluidic device concepts in a PDMS based microfluidic systems, in order to take advantage of merits of both PDMS and nanofluidics.

More recently, the demonstration of utilizing a PDMS microchannel for protein preconcentration has been carried out by Kim and co-workers, using spontaneous narrow channel underneath the wall between the PDMS and glass.[37] However, they utilize reversible bonding of PDMS to glass substrate, which is less robust than permanent, plasma-initiated bonding process widely accepted. This could make on-chip integration of fluidic component difficult.

In this article, we report a device that can achieve similar nanofluidic protein preconcentration as previously reported nanofluidic preconcentration systems, the fabrication of which only requires an extremely simple nanogap formation through two microchannels via breakdown junction gap formation. Nanogaps generated by this method show qualitatively the similar behavior as microfabricated regular nanochannels, and efficient protein concentration using the device has been demonstrated.

EXPERIMENTAL SECTION

Microchip fabrication

The microchip was fabricated using poly(dimethylsiloxane) (PDMS) (Sylgard 184, Dow Corning Inc., Midland, MI) bonded with commercial slide glass plate. The fabrication included three major steps: (1) master fabrication, (2) PDMS pouring/curing step, and (3) irreversible bonding to the slide glass plate via plasma treatment. As a first step, SU8 photoresist (SU8-2025, MicroChem Inc., Newton, MA) pattern on silicon was used as a master. The positive master mold for the device contained channels that are 50 μm wide and 20 μm deep. Master with SU8 photoresist was treated with a hexamethyldisilane (Sigma-Aldrich, St. Louis,

MO) for 1 h for preventing adhesion with PDMS. The hexamethyldisilane solution was evaporated on the master in a desiccator with a 5 psi vacuum. As a second step, PDMS was poured on the master mold, which was degassed in a desiccator with a 5 psi vacuum for 1 h before pouring. After curing in an oven at 65 °C for 3 h, the PDMS layer was peeled off from the silicon master. To punch holes through the end of the channels, we used a metal syringe needle with an outer diameter of 1/16 in. (Hamilton Co., Reno, NV). As a third step, PDMS and glass plate were treated with an oxygen plasma in a plasma cleaner (Harrick Plasma, Ithaca, NY) for 1 min, and immediately bonded PDMS to the glass substrate within 30 sec. After bonding, the two pieces were brought into conformal contact directly after removal from the plasma to form an irreversible seal and then the PDMS device was reheated in an oven at 60 °C for 12 h to increase the bonding strength.

Nanogap formation

After microchip fabrication, nanogaps were formed between microchannels via junction gap breakdown phenomenon. After filling 10^{-2} M phosphate (dibasic sodium phosphate, pH 9.1) buffer in all the channels, we applied the high voltage (1000 V) to initiate electrical breakdown onto two anodic side reservoirs, while others (cathodic side) were grounded (Fig. 1a). Here, the distance of junction gap between cathode and anode was 40 μm, and applied electrical field was 25 V/μm. Both BODIPY-disulfate (di-anion) from Molecular Probes and Rhodamine 6G (cation) from Sigma-Aldrich were used to observe nanogap formations via junction gap breakdown.

DC current measurement for the estimation of nanogap

The DC current measurements as a function of applied voltage (I-V curve) were carried out using a Keithley 236 Source/Measure Unit to investigate the nanogap formation and measure its dimension. Based on the study of Stein and coworkers[38] that ions transport in nanochannel is governed by surface charge at low buffer concentration, we mainly used relatively high concentration of 10^{-1} M potassium chloride (KCl) as a buffer solution for DC current measurement, providing the discrimination of nanogap depth.

The measurement of the nanogap width after junction gap formation is needed for measuring nanogap dimension that was formed by junction gap breakdown. We added 10^{-5} M BODIPY in 10^{-1} M KCl buffer solution to measure nanogap width from fluorescence images caused from the nonspecific adsorption of BODIPY dye onto PDMS surface during nanogap formation process.

Here, we used simple equivalent circuit model consisting of serial resistance. The resistance of microchannel was measured using the electrolyte solution mentioned above, corresponding to the Debye length of 0.96 nm.[39] A precision high-voltage power supply (model PS325, Standford Research Systems, Inc) was used to apply high voltage for junction gap breakdown voltage and then current measurements were carried out using Keisley 236 module. Note that Ag/AgCl electrode was used for the DC measurement to prevent overpontential. An Ag/AgCl electrode is well-known as a nonpolarizable electrode that current passes freely across the interface and therefore shows no overpotential. We applied voltage from 0.25 V to 1.5 V with 0.25 V step. The applied voltage was selected below 2 V to prevent bubble formation that might be generated above 2 V.

Materials and measurement set-up for preconcentration

A β-Phycoerythrin, a molecular weight of 240 kDa and a pI value of 4.3, from Sigma-Aldrich Chemical Co (St. Louis, MO) was mainly used to investigate the operating of protein preconcentration. Three different concentration of β-Phycoerythrin, 400 pM, 4 nM, 40 nM, was prepared using a 10^{-2} M phosphate buffer at pH 7.

In order to concentrate the protein, we initially applied 100V onto two anodic side reservoirs, while others were grounded. Then we applied V_1=100V and V_2=90V to balance two forces between anion repulsion from the space charge layer versus electroosmotic flow from the reservoir as suggested by previous reports.[15]

To observe the buffer pH dependence of electrokinetic trapping for the preconcentration, several different buffer solutions were used. For the buffer system of pH 4 and pH 5, acetate buffer, the mixture of acetic acid and sodium acetate, was used, while phosphate buffer was used from the mixture of dibasic sodium phosphate for pH 7 and pH 9. The pH measurement of each buffer was carried out using a pH meter (Corning, Scholar model 425).

An inverted epifluorescence microscope IX 51 (Olympus, Melville, NY) equipped with a thermoelectrically cooled CCD camera (Cooke Co., Auburn Hill, MI) was used for fluorescence imaging. Fluorescence images were analyzed using ImagePro software (Scanalytics, Fairfax, VA). A neutral density filter was used to prevent CCD array from saturation so that we can achieve the increasing of the dynamic range and the reducing of photobleaching effect.

RESULTS AND DISCUSSION

Nanogap formation using a junction gap electric-breakdown

The chip is composed of 3 microchannels, for a concentration device using simple PDMS layer molding and irreversible plasma bonding on glass without any micro/nano fabrication step (Fig. 1a). The simple chevron-shaped microchannel was designed to focus the electric field on the tip point, instead of two straight channels terminating near the horizontal channel[40], for facilitated breakdown generation. One channel is for an anodic channel (the parallel channel in the middle) and two are for cathodic channels (top and bottom chevron-shaped channels). The operation of preconcentration consists of simply two steps (Fig. 1a). The first step is nanogap formation using a junction gap electric-breakdown between microchannels by applying high voltages. After flushing microchannles using a pressure-driven flow (for removing bubbles that can be generated under high voltage), the preconcentration step using electrokinetic trapping method[15] is carried out to operate the device.

When high voltage is applied through junction gap, a nanogap is formed between two junctions of three microchannels (Figure 1b). We filled a mixture of 10^{-2} M phosphate (dibasic sodium phosphate, pH 9.1) buffer and a 10^{-5} M Rhodamine 6G positive dye to all the channels, and then an electric field of 25 V/μm is applied, which is slightly above the dielectric strength of PDMS (21 V/μm), across two microchannels. Rhodamine 6G was used for the clear observation of nanochannel formation via adsorption of positive dye onto a PDMS surface.

The suggested mechanism of nanogap formation via junction gap breakdown is as follows; initially, a depletion layer is formed on anodic side and propagation starts from the anodic to cathodic side (t_0 in Fig. 1b). Nanopores in a junction gap, distributed on PDMS materials with nanometer size, might lead to the formation of an initial depletion layer under high voltage according to the exclusion-enrichment effect (EEE). The PDMS/glass interface, which has finite roughness and improper bonding, would be another possible explanation about the formation of an initial depletion. Then the depletion layer on the anodic side expands parallel to anodic channel direction and a nanogap propagates normal to the anodic channel direction (t_1 in Fig. 1b). Finally, the propagation of a nanogap starting from the anodic side contacts the cathodic channel (ground channel) and then both the depletion layer and the nanogap width increase as a function of time (t_2 in Fig. 1b). We observed a similar breakdown pattern in the case of using 10^{-5} M BODIPY as a negative dye in 10^{-2} M phosphate buffer. Eventually, the

trapezoidal nanogap structure was formed between two microchannels, which can act as a permselective membrane.

Estimation of the nanogap dimension using DC current measurement

The conductivity of a rectangular-shaped nanogap has been previously investigated by Stein and co-workers.[38] They observed that a significant saturation of conductance occurred at low ionic strength regardless of nanogap size due to large Debye layer effects. For an estimation of the nanogap dimension, we carried out the DC current measurement using relatively high concentration of KCl electrolyte at 10^{-1} M, which corresponds to the very thin, non-overlapping electrical double layer (EDL) before and after the nanogap formation. The resistivity of 10^{-1} M KCl electrolyte was reported as 0.83 Ωm.[41] Note that a simple equivalent circuit model was used for the estimation of nanogap depth as depicted as Figure 2(a). Each microchannel branch can be defined as the resistor which has a value of R_m, while the nanogap has R_n, and the length of all the branches of microchannel was 5 mm.

Line 1 in Figure 2(b) indicates the I-V curve through upper microchannels which is consisted of two parallel resistors of $R_{m\ (\text{left channel})}$ and $R_{m\ (\text{right channel})}$. The line 1 was measured for the reference in the calculation of nanogap depth. The I-V curve shown in Line 2 was measured through two electrodes (upper-left one and center-right one) which have the resistors of $R_m + R_n + R_m$ after nanogap formation. In the absence of nanogap (Line 3; before nanogap formation), R_n showed almost infinite value up to 1.5V and no passing current through microchannels was observed.

From above plots, we can measure the slope of each curve (s_1 and s_2) and the relationship between the slope and resistance is

$$\frac{1}{s_1}=R_m+R_m, \quad \frac{1}{s_2}=R_m+R_n+R_m. \tag{1}$$

Then, the DC resistance of a fluid in nanogap can be computed as

$$R_n=\frac{1}{s_2}-\frac{1}{s_1}=\rho\frac{L_n}{W_nD_n}, \tag{2}$$

where ρ is the resistivity of buffer electrolyte, L_n, W_n and D_n are the nanogap length, width and depth, respectively under assumption of the nanogap is rectangular shape. Therefore, the effective depth of nanogap can be calculated by

$$D_{\text{eff(nanogap)}}=\rho\frac{L_n}{W_n}\left(\frac{1}{s_2}-\frac{1}{s_1}\right)^{-1}. \tag{3}$$

The length and width of nanogap can be determined by experimental observation. In order to quantify a nanogap depth from the I-V curve, we added 10^{-5} M BODIPY dye in 10^{-1} M KCl solution so that we could measure the width of nanogaps from fluorescence images (see t_2 image in Fig. 1b). Here, the width from measurement was 28 μm, and length of the nanogap was 40 μm from fixed junction gap size.

The increase of the I-V slope after nanogap formation (line 2) compared with that from before one (line 3) corresponds to the decrease of electrical resistance, therefore indicating the nanogap formation at the junction. From the data in Figure 3b using 25 V/μm breakdown voltages, experimentally estimated effective nanogap depth is approximately 80 nm. The experimental data in Figure 2 show the average values of five devices and it reveals a coefficient of variation (C.V.) of less than 6%. Apparently, we acquired reproducible nano-meter scale gap between microchannels by junction gaps breakdown, although conductance in such a thin nanogap might not be correctly characterized by the model we used.

Protein preconcentration using the nanogap

Preconcentration of β-phycoerythrin (β-PE) protein as a function of time for three different concentration (400 pM, 4 nM, and 40 nM) was shown in Figure 3a. Center channel is filled with β-PE protein in 10 mM phosphate buffer (pH 7), and two chevron-shaped microchannels are filled with 10 mM phosphate buffer solution. The preconcentration from three different initial concentrations was conducted for 60 min to verify the linearity and stability. We have used electrokinetic trapping method in the anodic side of the nanogap, as done in our previous publication and [15] the experimental data in Figure 3 show the average values of five devices. The concentration of collected β-PE protein from fluorescence intensity was averaged over a rectangular window (5 min image in Fig. 3b). To calculate final concentration, the fluorescence intensity of the standard sample solutions (2, 4, 8 μM) was measured. The result shows that the preconcentration factors up to 10^4 have been achieved within 60 min. From fluorescence images from 4 μM initial concentration (Fig. 3b), both the signal intensity and volume of protein concentration quite stably increased with time (See the supplement animation). The parabolic shape of the preconcentrated plug is most likely from small, residual background flow in the microchannel, caused by minute reservoir level height differences and/or surface tension differences. The observed volume of preconcentration is as high as 70 pL in 60 min collection, which are 120 folds larger than that from our previous reports.[15] The time evolution of concentration plugs for different cases show different slopes, which was the behavior common to earlier preconcentration experiments[15, 37]. The reason for this behavior is unclear, while it seems to be related to many factors including diffusivity, (nonlinear) convection within the plug, and non-specific binding of molecules to the wall. The location of concentrated plug is behind the ion depletion zone, which is in line with our earlier results using Si-based nanofluidic preconcentration systems. This type of preconcentration is occurring only on the anodic side (where ion depletion occurs), which is different from enrichments (occurs at cathodic side).

The buffer pH effect on electrokinetic trapping for the preconcentration of β-PE protein is shown in Figure 4. For the pH effect, the β-phycoerythrin proteins were diluted using different buffers. Acetate buffer was used as pH 4 and pH 5 buffer systems, and phosphate buffer, mixture of monobasic and dibasic sodium phosphate, was used as pH 7 and pH 9 buffer systems. Note that the pI of β-phycoerythrin protein is ~ 4.3. At the pH conditions well above the pI value of the protein (Fig. 4a~4c), β-phycoerythrin molecules were collected proportionally with time, while at pH 4 (Fig. 4d), the collection of β-phycoerythrin is not observed due to significant protein adsorption on PDMS nanogap. This non-specific adsorption is an irreversible process and results in the decrease of zeta potential (permselectivity) in nanogap. Both the fluorescent volume and the intensity of preconcentration noticeably increased as buffer pH (above the pI of β-phycoerythrin protein) is increased. In the higher buffer pH conditions, proteins have larger number of negative charge, which leads to faster collection by electrokinetic trapping. We also suggest that the higher efficiency at high pH conditions comes from the increase of tangential force (electroosmotic flow through microchannel) in higher pH, which comes from the increase of zeta potential at higher pH buffer range. From these results, we can demonstrate that the protein preconcentration can be acquired under several different buffers (phosphate, acetate) at several different pH values (pH 5~pH 9).

CONCLUSION

Using only a soft lithography and PDMS microfluidics, we developed a nanofluidic protein preconcentrator with larger concentration volumes than that from our previous preconcentration results using Si-glass materials. [21] Nanogaps with a permselectivity can be formed by an electrical breakdown through a gap junction between two PDMS microchannels. The preconcentration device with a simple fabrication can be incorporated into various existing

PDMS microfluidic systems architecture without major technical issues. The fabrication of large volume concentration device is crucial for the preconcentration application of protein/peptide, since the commercial analytical system such as mass spectroscopy (MS) or MS/MALDI (Matrix-assisted laser desorption/ionization) requires large sample plugs (from nanoliter to microliter). In addition, similar PDMS-based nanofluidic devices could be useful to combine the benefits of flexible PDMS materials with novel nanofluidic device concepts.

Supplementary Material

Refer to Web version on PubMed Central for supplementary material.

ACKNOWLEDGEMENT

This work was supported by the NIH Grant (NIBIB, EB005743). J. Han was partially supported by NSF CAREER (CTS- 0347348) program. J. H. Lee was partially supported by Korea Research Foundation grant (KRF-2005-000-10051-0). S. J. Kim was partially supported by Samsung Electro Mechanics Postdoctoral program. Microfabrication of the device was done in the Microsystems Technology Laboratories of MIT, with the help of its staff members.

REFERENCES

1. Burns MA, Johnson BN, Brahmasandra SN, Handique K, Webster JR, Krishnan M, Sammarco TS, Man PM, Jones D, Heldsinger D, Mastrangelo CH, Burke DT. Science 1998;282:484–487. [PubMed: 9774277]
2. Harrison DJ, Fluri K, Seiler K, Fan ZH, Effenhauser CS, Manz A. Science 1993;261:895–897. [PubMed: 17783736]
3. Lichtenberg J, Verpoorte E, de Rooij NF. Electrophoresis 2001;22:258–271. [PubMed: 11288893]
4. Burgi DS, Chien RL. Anal. Chem 1991;63:2042–2047.
5. Jung B, Bharadwaj R, Santiago JG. Anal. Chem 2006;78:2319–2327. [PubMed: 16579615]
6. Gebauer P, Bocek P. Electrophoresis 2002;23:3858–3864. [PubMed: 12481281]
7. Oleschuk RD, Shultz-Lockyear LL, Ning YB, Harrison DJ. Anal. Chem 2000;72:585–590. [PubMed: 10695146]
8. Yu C, Davey MH, Svec F, Frechet JMJ. Anal. Chem 2001;73:5088–5096. [PubMed: 11721904]
9. Kutter JP, Jacobson SC, Ramsey JM. J. Microcolumn Sep 2000;12:93–97.
10. Ross D, Locascio LE. Anal. Chem 2002;74:2556–2564. [PubMed: 12069237]
11. Wang Y-C, Choi MH, Han J. Anal. Chem 2004;76:4426–4431. [PubMed: 15283583]
12. Cui H, Horiuchi K, Dutta P, Ivory CF. Anal. Chem 2005;77:7878–7886. [PubMed: 16351133]
13. Pu Q, Yun J, Temkin H, Liu S. Nano Lett 2004;4:1099–1103.
14. Foote RS, Khandurina J, Jacobson SC, Ramsey JM. Anal. Chem 2005;77:57–63. [PubMed: 15623278]
15. Wang YC, Stevens AL, Han JY. Anal. Chem 2005;77:4293–4299. [PubMed: 16013838]
16. Han J, Craighead HG. Science 2000;288:1026–1029. [PubMed: 10807568]
17. Li J, Stein D, McMullan C, Branton D, Aziz MJ, Golovchenko J. Nature 2001;412:166–169. [PubMed: 11449268]
18. Kasianowicz JJ, Brandin E, Branton D, Deamer DW. Proc. Natl. Acad. Sci. U.S.A 1996;93:13770–13773. [PubMed: 8943010]
19. Foquet M, Korlach K, Zipfel W, Webb WW, Craighead HG. Anal. Chem 2002;74:1415–1422. [PubMed: 11922312]
20. Turner SW, Perez AM, Lopez A, Craighead HG. J. Vac. Sci. Technol. B 1998;16:3835–3840.
21. Harnett CK, Coates GW, Craighead HG. J. Vac. Sci. Technol. B 2001;19:2842–2845.
22. Nam, W. Bae, J; S; Kalkan, AK.; Fonash, SJ. J. Vac. Sci. Technol. A 2001;19:1229–1233.
23. Czaplewski DA, Kameoka J, Mathers R, Coates GW, Craighead HG. Appl. Phys. Lett 2003;83:4836–4838.

24. Melechko AV, McKnight TE, Guillorn MA, Merculov VI, Ilic B, M. Doktycz J, D. Lowndes H, Simpson ML. Appl. Phys. Lett 2003;82:976–978.
25. Mao P, Han J. Lab Chip 2005;5:837–844. [PubMed: 16027934]
26. Haneveld J, Jansen H, Berenschot E, Tas N, Elwenspoek M. J. Micromech. Microeng 2003;13:S62–S66.
27. Hibara A, Saito T, Kim HB, Tokeshi M, Ooi T, Nakao M, Kitamori T. Anal. Chem 2002;74:6170–6176. [PubMed: 12510735]
28. Wang YM, Tegenfeldt JO, Reisner W, Riehn R, Guan X-J, Guo L, Golding I, Cox EC, Sturm J, Austin RH. Proc. Natl. Acad. Sci. U.S.A 2005;102:9796–9801. [PubMed: 15994229]
29. Campbell LC, Wilkinson MJ, Manz A, Camilleri P, Humphreys CJ. Lab Chip 2004;4:225–229. [PubMed: 15159783]
30. Volkmuth WD, Austin RH. Nature 1992;358:600–602. [PubMed: 1501715]
31. Gogotsi Y, A.Libera J, Yazicioglu AG, Megaridis CM. Appl. Phys. Lett 2001;79:1021–1023.
32. Chou SY, Krauss PR. Microelectron. Eng 1997;35:237–240.
33. Guo LJ, Cheng X, Chou C-F. Nano Lett 2003;4:69–73.
34. Quake SR, Scherer A. Science 2000;290:1536–1540. [PubMed: 11090344]
35. McDonald JC, Whitesides GM. Acc. Chem. Res 2002;35:491–499. [PubMed: 12118988]
36. Unger MA, Chou H-P, Thorsen T, Scherer A, Quake SR. Science 2000;288:113–116. [PubMed: 10753110]
37. Kim SM, Burns MA, Hasselbrink F. Anal. Chem 2006;78:4779–4785. [PubMed: 16841895]
38. Stein D, Kruithof M, Dekker C. Phys. Rev. Lett 2004;93No. 035901-1
39. Probstein, RF. Physicochemical hydrodynamics: an introduction. New York: John Wiley & Sons Inc; 1994.
40. Horiuchi K, Dutta P. Lab Chip 2006;6:714–723. [PubMed: 16738721]
41. Morgan, H.; Green, NG. AC electrokinetics: colloids and nanoparticles. England: Research studies press Ltd; 2003.

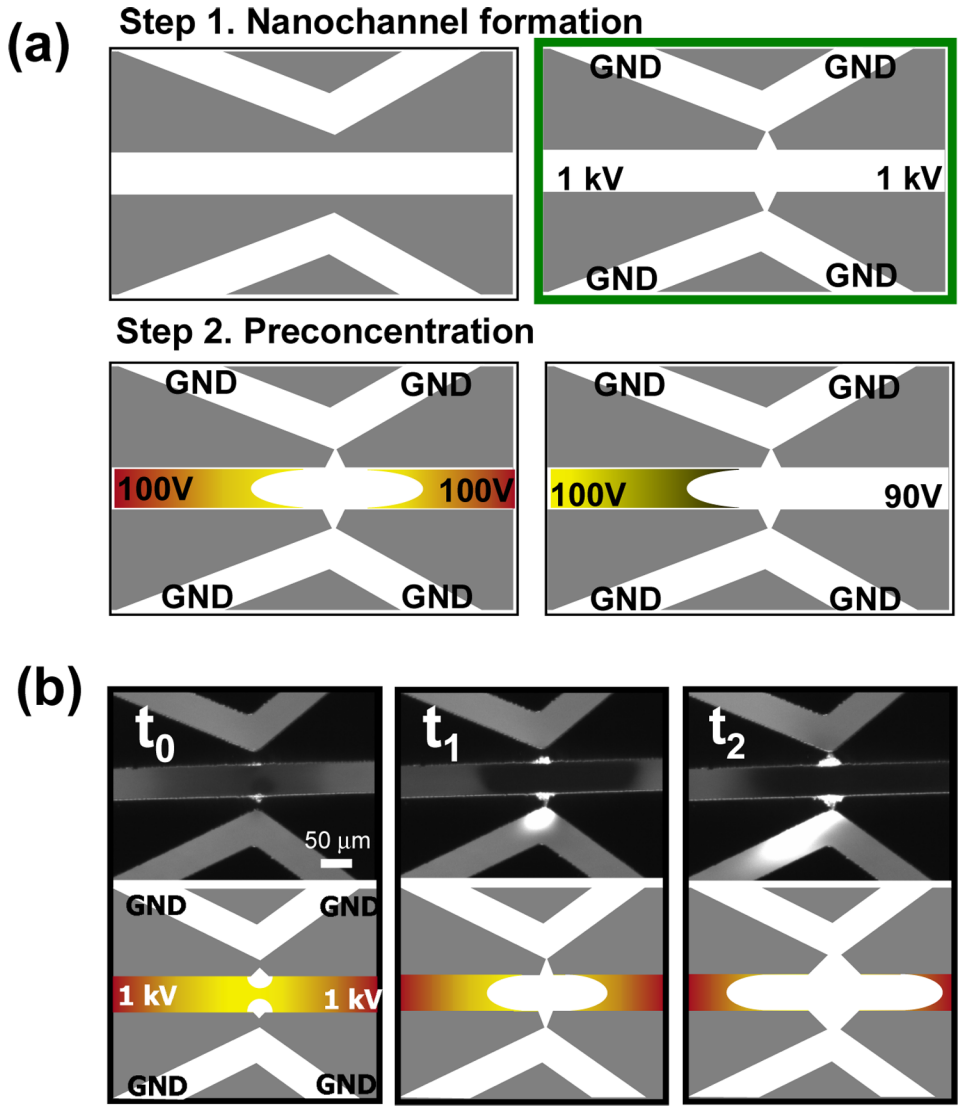

Figure 1.
Junction gap nanochannel formation and preconcentration operation. (a) Schematic diagrams for nanogap formation and preconcentration steps. (b) Time-evolutioni of junction gap breakdown process. We applied the high electrical field of 25 V/μm across two microchannels and acquired the trapezoidal nanogap structure between two microchannels which can act as permselective membrane.

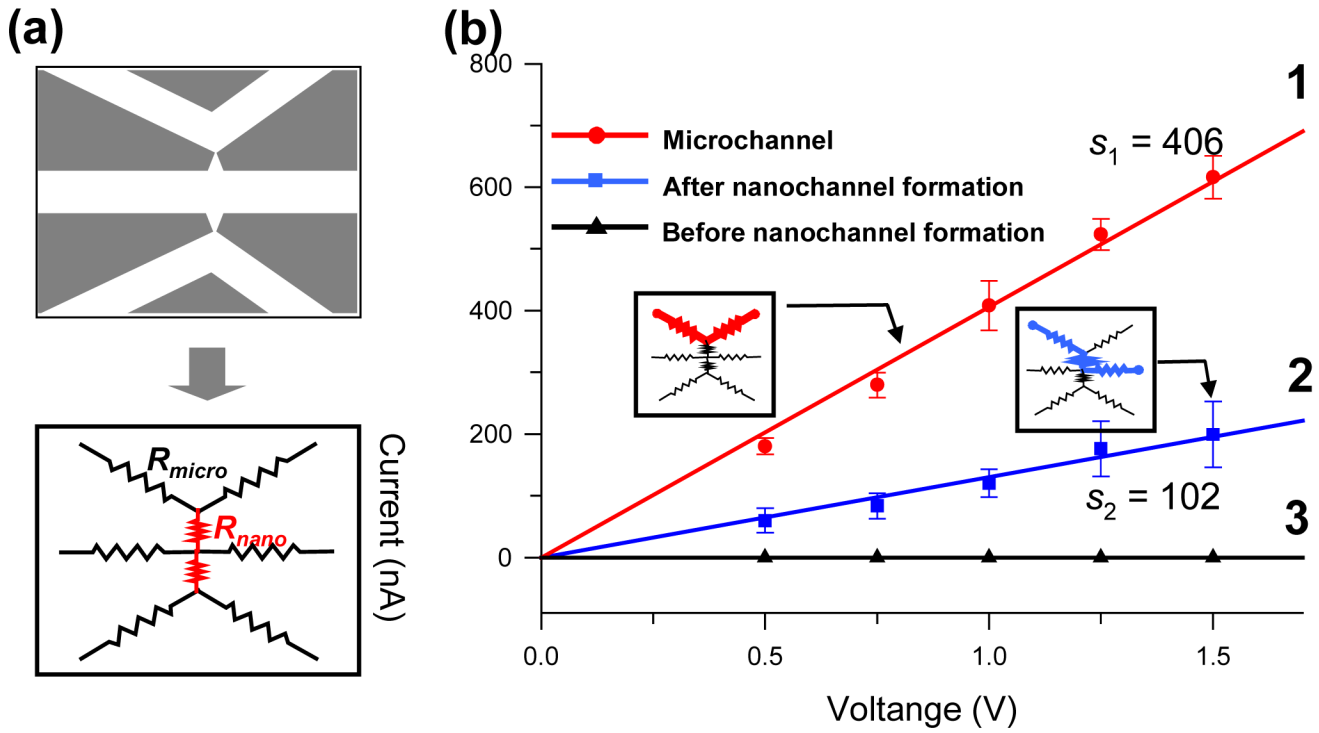

Figure 2.

I-V curves for the estimation of nanogap depth. (a) Simple equivalent circuit for the depth estimation. (b) The I-V curve before and after nanogap formation. Line 1 indicates I-V curve of microchannel ($R_{m(left\ channel)}$+$R_{m(right\ channel)}$) for the reference in the calculation of nanogap depth. Line 2 indicates the I-V curves measured after nanogap formation, while line 3 reveals before nanogap formation. Form simple I-V slope, we calculated nanogap size via simple equivalent circuit model of serial resistance. Experimental nanogap depth in here is approximately 80 nm.

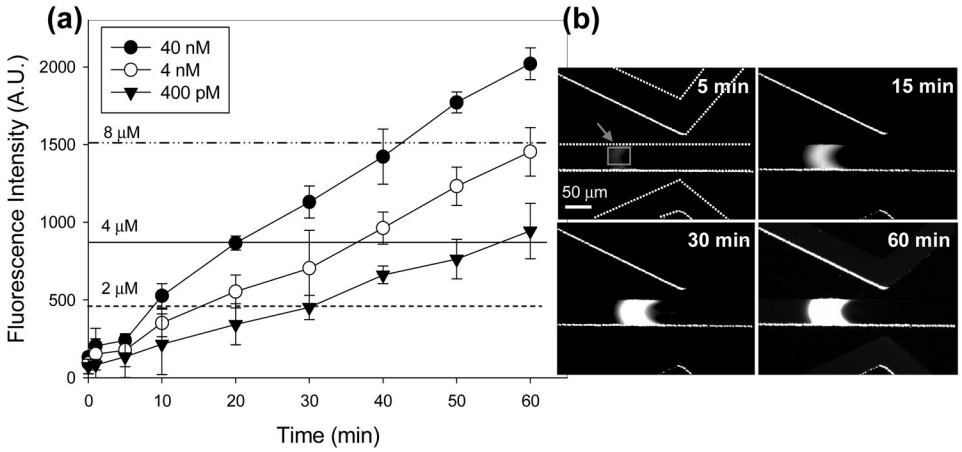

Figure 3.

(a) Preconcentration of β-phycoerythrin protein (β-PE) as a function of time up to 60 min for three different concentrations, showing the preconcentration factor of $>10^4$. (b) Time sequence of fluorescence image taken from 4 nM β-PE protein in 10 mM phosphate buffer solution (pH 7.0). Fluorescence images reveal that the preconcentration of proteins increase in both size and concentration with time. The volume of preconcentration is as high as 70 pL after 60 min collection.

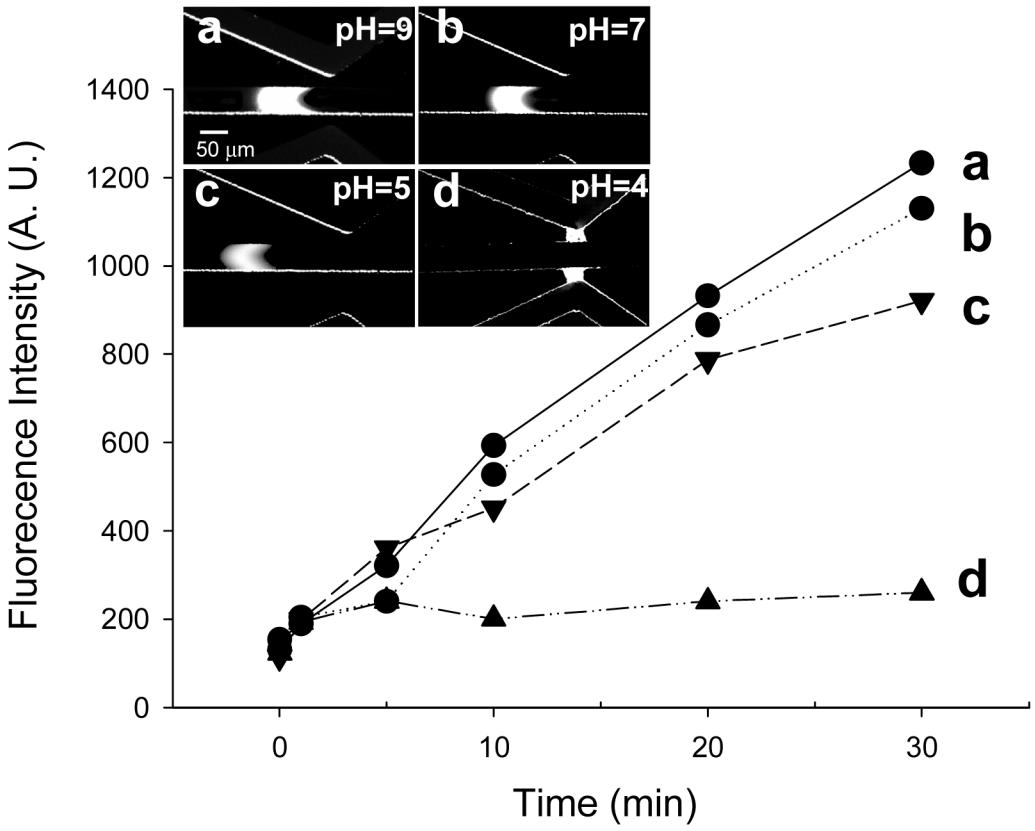

Figure 4.

The buffer pH effect on electrokinetic trapping for the preconcentration of β-PE protein after 30 min collection. Note that the pI of β-phycoerythrin protein is ~ 4.3. Above pI values (pH 5–9), negative charged protein collected proportional with time, while in pH 4, the collection of positive protein is not observed due to positive protein adsorption on PDMS nanogap.